

GHGT-12

CO₂ Exsolution – Challenges and Opportunities in Subsurface Flow Management

Lin Zuo^{a*}, Sally M. Benson^a

^a*Department of Energy Resources Engineering, Stanford University, Stanford, California, U.S.A.*

Abstract

This paper summarizes the results of a 4-year study regarding the implications of CO₂ exsolution on geological carbon storage security and subsurface flow management, including core-flood experiments, micro-model studies, pore-scale modeling, and relative permeability calculations. When separate phase CO₂ exsolves from carbonated water in sandstones, water relative permeability drops significantly. The relative permeability of exsolved CO₂ is disproportionately reduced compared to drainage due to the dispersed morphology of exsolved CO₂ bubbles in the pore space. Our studies suggest that CO₂ exsolution provides an opportunity for mobility control in subsurface processes. The low mobility of exsolved CO₂ suggests that risks of groundwater contamination due to this phenomenon are small.

© 2014 The Authors. Published by Elsevier Ltd. This is an open access article under the CC BY-NC-ND license (<http://creativecommons.org/licenses/by-nc-nd/3.0/>).

Peer-review under responsibility of the Organizing Committee of GHGT-12

Keywords: CO₂ exsolution; relative permeability; capillary trapping; depressurization

1. Introduction

Carbon dioxide is known to be highly soluble in water/brine, up to 5% mass fraction under reservoir conditions. In geological carbon sequestration, a large fraction of the injected CO₂ will dissolve in brine over time. While dissolved CO₂ presents a much lower release risk compared to free phase CO₂ [1,2], the risk is not zero. Exsolution occurs when pore pressures decline and CO₂ solubility in brine decreases, resulting in the formation of a separate CO₂ phase [3-6]. This scenario occurs in carbon sequestration reservoirs by upward migration of CO₂ saturated brine, through faults, leaking boreholes or even seals, driven by the upward pressure gradient from CO₂ injection or ground water extraction [7,8]. In this way, dissolved CO₂ could migrate out of storage reservoir and form a gas phase at shallower depths.

* Corresponding author. Currently at Chevron Energy Technology Company, USA. E-mail address: linzuo@chevron.com.

The most important question is whether CO₂ exsolution creates significant risks for carbon storage security. Answering this question requires knowledge of the mobility of exsolved CO₂ and its influence on subsurface flows. First, we present relative permeability measurements during CO₂ exsolution in sandstone cores and compare them to measurements during drainage and imbibition. Then, we develop a model with the knowledge obtained from experimental observations to simulate the growth and morphology of exsolved CO₂ bubbles in digital rock volumes based on X-ray CT images. This calibrated model predicts gas distribution and morphology over a range of conditions. A Stokes flow simulator is used to calculate fluid flows in porous media that contain exsolved CO₂, and estimate the water relative permeability curves in various sedimentary rocks and reservoir conditions.

2. Relative Permeability Measurements

Core flooding experiments are conducted to measure relative permeabilities of exsolved CO₂ and water during exsolution. These data are compared to measurements during drainage to investigate how exsolved CO₂ behaves differently. Table 1 summarizes properties of the Berea sandstone, Sa'ad sandstone and Mt. Simon sandstone used in this study. The experimental setup enables steady-state measurements of relative permeability for the CO₂-water system [9]. Comparison between the relative permeability curves for exsolution [4] and drainage [10] for Sample 1 (Berea sandstone) are shown in Figure 1. For exsolved CO₂, the relative permeability is in a range of 10⁻⁵ to 10⁻³ for CO₂ saturations of 10~40%. For the water phase, the relative permeability drops dramatically as CO₂ exsolves, compared to drainage. After drainage or exsolution, CO₂ saturated water is injected into the sample for an imbibition process. Figure 2 shows the measured water relative permeabilities at imbibition endpoints in the Berea sandstones and the Mt. Simon sandstone. With Sample 2, similar initial CO₂ saturations are created before imbibition (20% with CO₂ injection and 18% with exsolution). Water is injected at a rate of 15 mL/min (Ca≈10⁻⁶) during imbibition. The water relative permeability is 0.28 at 16% gas saturation in the post-drainage measurement and 0.65 at 10% gas saturation in the post-exsolution measurement. The water relative permeability with exsolved CO₂ is less than half of the value with injected CO₂.

Table 1. Rock properties and experimental conditions.

Sample	Rock Name	Permeability/md	Porosity	Length/cm	Preparation
1	Berea	1066	22.7	10.2	Heated at
2	Berea	507	19.9	14.8	700°C for
3	Berea	470	19.0	16.5	12-16 hours
4	Berea	18	16.5	17.5	before
5	Berea/Sa'ad	510/0.3	19.7/6.2	11.4/1.3	experiments
6	Mt. Simon	15.7	23.9	9.0	Dried at 50°C

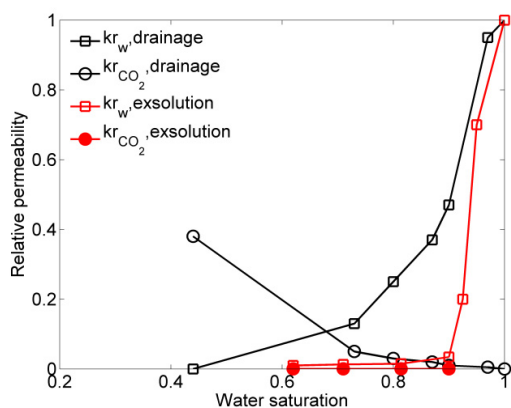


Fig. 1. Comparison of water and exsolved CO₂ relative permeability curves between exsolution [4] and drainage [10] measured with Sample 1.

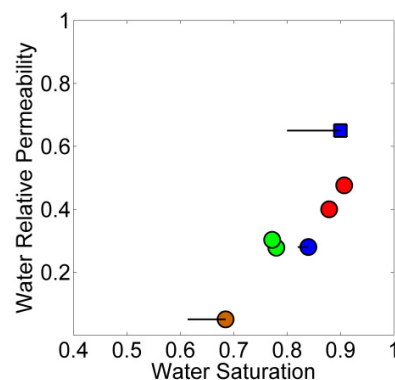


Fig. 2. Water relative permeability measured at imbibition endpoints in Sample 2 (blue), 3 (green), 4 (red) and 6 (brown). Post-exsolution measurements are circles, and the post-drainage measurement is square. Horizontal lines on markers denote the pre- and post-imbibition CO₂ saturations.

These experiments show that the water flow is strongly influenced by the presence of exsolved CO_2 , not only during exsolution, but also during post-exsolution imbibition. The influence of exsolved CO_2 on the water mobility is larger than for CO_2 introduced into the pore space by drainage.

3. Modeling and Flow simulation

3.1. Gas growth modeling

A gas growth model is developed to study the influence of depletion rate, rock geometry and mass transfer on the morphology of exsolved CO_2 . In the model, we assume randomly distributed bubble nucleation sites on the grain surfaces. The growth of individual bubbles is modeled explicitly, by decomposing bubble interfaces into spherical surfaces. Bubbles grow by advancing spherical surfaces along the least capillary pressure direction. We developed two conceptual scenarios: (1) the growth of gas is controlled by pure diffusion, referred to as the diffusion-controlled scenario; (2) mass transfer in the aqueous phase is enhanced by convection, referred to as the transport-enhanced scenario. In the diffusion-controlled scenario, growth of individual bubbles is not affected by neighboring bubbles while in the transport-enhanced scenario only bubbles in locations with high transport rates grow and bubbles with the least capillary pressure grow first.

Figure 3 shows results from modeling gas exsolution in a micro-model compared to experimental data (right) [5]. Here we model the growth of only one bubble observed at the center. The modeled result (left) demonstrates the progressive growth of this bubble under capillarity and matches well with the observation. Bubble growth models for three-dimensional pore geometries obtained for Domengine, Boise and Berea sandstones were also developed. Modeling domains are digitally re-constructed volumes from X-ray micro-tomography with $4.4 \mu\text{m}$ resolution. Figure 4 shows the modeled exsolved CO_2 distributions (15% saturation) in the Domengine sandstone sample with different nucleation fractions. Nucleation fractions, defined as the number of activated nuclei per unit grain surface area, are modeled as a power law function of the pressure depletion rate [11]. As shown in Figure 4, exsolved gas ganglia have a smaller average size and are less connected as the nucleation fraction increases.

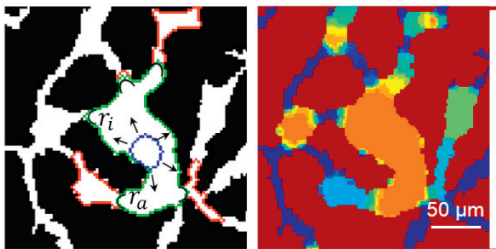


Fig. 3. Results from two-dimensional modeling of gas exsolution and comparison to experimental observation in a micro-model (right) [5].

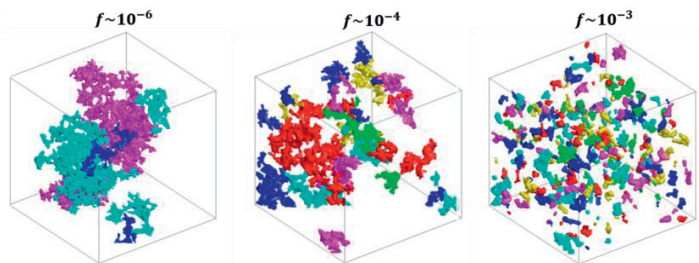


Fig. 4. Gas bubble distributions for modeling of gas exsolution in a Domengine sandstone with different nucleation fractions at a 15% CO_2 saturation.

Observation of exsolved gas distributions from X-ray microtomography (Beamline 8.3.2 at the Advanced Light Source, operated by Lawrence Berkeley National Laboratory) shows nuclei are most likely to grow in pores and throats with high flow rates. We attribute this to favorable convective transfer in the aqueous phase, especially in the early stage of gas growth. Modeled gas distributions in the transport-enhanced scenario replicate this feature and match experimental observations. Figure 5 shows modeled (shaded) and experimental (bars) ganglion size distributions for exsolved CO_2 in the Domengine sample for both scenarios. While most ganglia have similar sizes in the diffusion-controlled scenario with each nucleation fraction, variations of the modeled ganglia size in the transport-enhanced scenario are larger and match the experimental observations better. Modeled distributions with a 10^{-3} nucleation fraction appear to match experimental observations best.

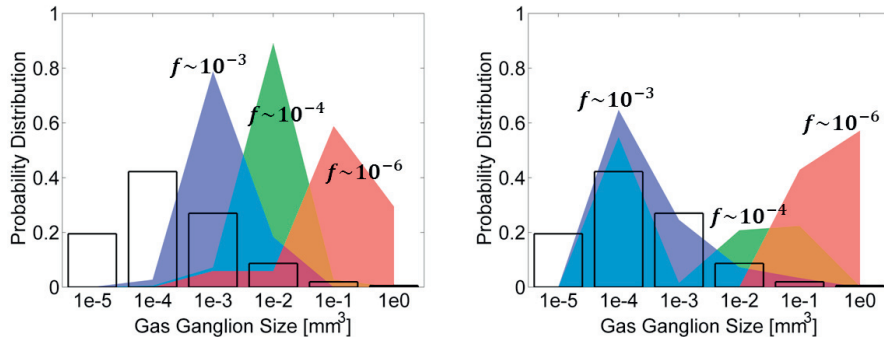


Fig. 5. Modeled (shades) and experimental (bars) ganglion size distributions of exsolved CO₂ in the Domengine sandstone in the diffusion-controlled scenario (left) and in the transport-enhanced scenario (right).

3.2. Stokes flow simulation and water relative permeability calculations

A Stokes flow simulator is used to estimate water relative permeability curves with exsolved CO₂ in various reservoir conditions and rocks. Formulation of the Stokes flow simulator is based on the approach taken by Silin and Patzek [12]. Computational domains are digital rock volumes measured using tomographic imaging (500×500×500, 4.4 μm voxel size for the Domengine and Boise sandstones, 1.8 μm for the Berea sandstone). We calculate water relative permeability curves with the presence of exsolved CO₂ as follows: (1) calculate the absolute permeability of a rock volume without gas; (2) generate realizations of exsolved CO₂ distributions in the rock volume with up to 35% gas saturation (10 realizations with each nucleation fraction); (3) calculate the effective permeabilities of the rock volume with 5%, 15%, 25% and 35% gas saturations for each realization. Assumptions in computing water relative permeability with CO₂ exsolution are: (1) the rock is water-wet; (2) capillary pressure determines the fluid distribution; and (3) exsolved gas is immobile. Zuo et al. [5] found that an exsolved gas saturation of 30~35% statistically characterizes when the CO₂ becomes mobile. As a result, voxels occupied by exsolved CO₂ are treated as solid grains and no CO₂ movement is allowed when the exsolved CO₂ saturation is less than 35%. Calculations of the water relative permeability are made between 0~35% gas saturation.

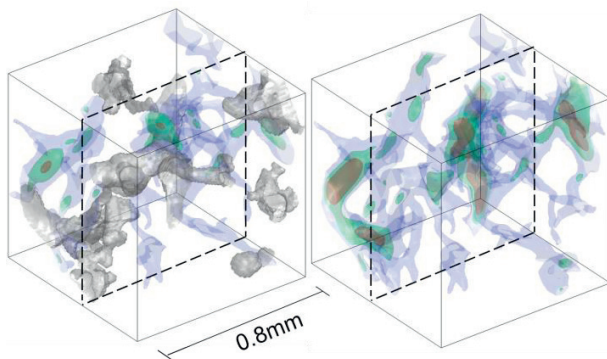


Fig. 6. Isosurfaces of simulated velocity fields in a portion of the Domengine sandstone sample, w/ (left) and w/o (right) exsolved CO₂ (gray). Blue/green/red surfaces are 10%, 50% and 80% of maximum velocity.

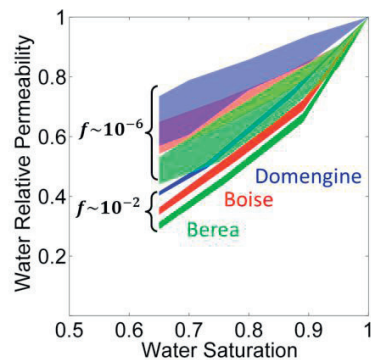


Fig. 7. Variations of calculated water relative permeability curves at different nucleation fractions in the diffusion-controlled scenario. Shaded area represents average value ± one standard deviation of ten gas distribution realizations (Domengine: blue; Boise: red; Berea: green).

The impact of exsolved CO₂ on the velocity field can be seen on Figure 6. Comparison between the two velocity fields clearly demonstrates that exsolved CO₂ clogs some of the water flow paths and reduces the overall flow.

Figure 7 shows the calculated water relative permeability curves for the diffusion-controlled scenario in the Domengine sandstone (blue), Boise sandstone (red) and Berea sandstone (green) samples. Each graph shows relative permeability for two nucleation fractions (10^{-2} and 10^{-6}). The shaded area represents the variation of calculated relative permeability values for ten realizations (average value \pm one standard deviation). As the nucleation fraction increases, more but smaller ganglia evolve in the rock volume, and the flow of water is further hindered by gas ganglia blocking more flow paths. Also, variations (or uncertainties) of calculated water relative permeabilities among realizations is reduced as the nucleation fraction increases, indicating a similar gas morphology forms regardless where nuclei initiate if the nucleation fraction is large enough.

Figure 8 shows the comparison of calculated water relative permeability curves between the diffusion-controlled scenario (w/o markers) and the transport-enhanced scenario (w/ markers). Calculated curves with two nucleation fractions (10^{-2} : solid curves; 10^{-6} : dash curves) are shown for each sample. For all three samples, water relative permeability curves in the transport-enhanced scenario are much lower compared to those in the diffusion-controlled scenario. Also, while the water relative permeabilities in the diffusion-controlled scenario reduce rather linearly with gas saturations, the water relative permeabilities in the transport-enhanced scenario drop dramatically with 5~10% gas saturations and drop moderately at higher gas saturations. This is caused by preferential gas growth in the pore space with high transport rates in the transport-enhanced scenario, which effectively reduces the water flow with a minimal amount of exsolved gas.

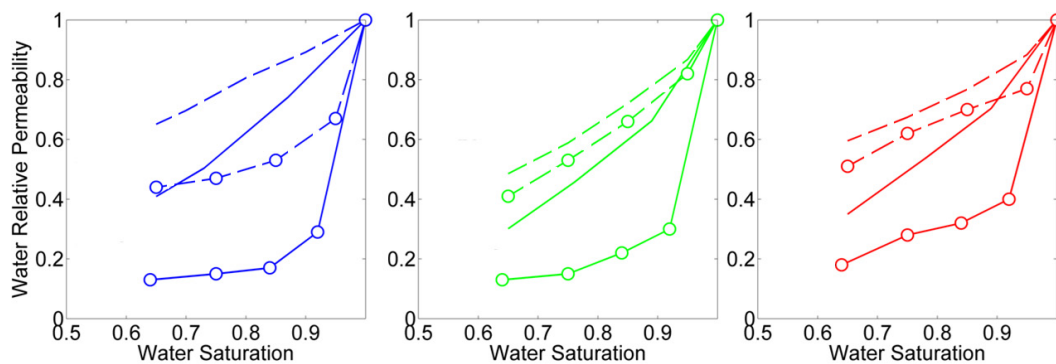


Fig. 8. Comparison of calculated water relative permeability curves at different nucleation fractions in the diffusion-controlled scenario (w/o markers) and the transport-enhanced scenario (w/ markers). Domengine sandstone: blue; Boise sandstone: red; Berea sandstone: green. Two nucleation fractions (10^{-2} : solid curves; 10^{-6} : dash curves) are shown.

Figure 9 shows the comparison between calculated water relative permeability curves using the Berea sandstone pore geometry and measurements from core-scale exsolution experiments. The measured water relative permeabilities are all within the range predicted by the diffusion-controlled and transport-enhanced scenarios, but are closer to the transport-enhanced curve. This suggests in our core-scale experiments, the exsolution process is enhanced by convective transfer in the aqueous phase. With a pressure depletion rate between 0.1 and 1 MPa/hr, the nucleation fraction is estimated to be approximately 10^{-2} , based on modeled gas phase morphology and relative permeability of the wetting phase. According to Tsimpanogiannis and Yortsos [11], the nucleation fraction is a power law of the depletion rate and the exponent is close to one unless the depletion rate is extremely slow. Therefore, we can extrapolate our results to reservoir conditions where the pressure decline rate is likely to be much slower than our experiments. If the depletion rate is 5 kPa/day for a reservoir of carbonated water, the nucleation fraction should be approximately $10^{-6} \sim 10^{-5}$. According to our calculations, with only 5% exsolved gas, the water relative permeability will be 0.67 in the Domengine sandstone, 0.77 in the Boise sandstone and 0.82 in the Berea sandstone.

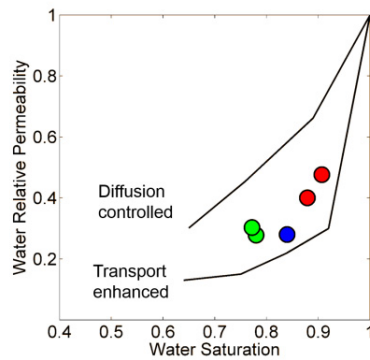


Fig. 9. Comparison of calculated water relative permeability curves with 10^{-2} nucleation fraction in the Berea sandstone image and measurements (circles) in the core-scale exsolution experiments with Berea sandstone Sample 2 (blue), 3 (green) and 4 (red).

4. Conclusions

Experiments, theory, and simulation are used to study the impact of CO_2 exsolution on storage security. Major findings are summarized below.

Exsolved CO_2 has extremely low relative permeability in sedimentary rocks. Measured exsolved CO_2 relative permeabilities are in a range of $10^{-5} \sim 10^{-3}$, even when the exsolved CO_2 saturation increases to over 40% during exsolution. Compared with the continuous and connected flow paths established by the CO_2 phase introduced drainage, exsolved CO_2 is poorly interconnected and spatially evenly distributed.

The presence of exsolved CO_2 disproportionately reduces the relative permeability to water compared to CO_2 introduced by drainage. Core scale measurements show the water relative permeability drops below 0.2 with only 5~15% exsolved CO_2 saturations. During a sequential imbibition, the water relative permeability with exsolved CO_2 is less than half of the measured value with CO_2 introduced by pre-imbibition drainage.

Convective transfer in the aqueous phase plays an important role in bubble growth and accumulation during exsolution. For carbonated brine migrating up a fault from a carbon storage reservoir, the growth of exsolved CO_2 will be largely supported by convection of brine from below. Experimental results show that exsolved gas is more likely to form and accumulate at locations with large water velocities. We develop a bubble nucleation and growth model, in which two mass transfer scenarios are considered: a diffusion-controlled scenario, where gas growth is controlled by pure diffusion, and a transport-enhanced scenario, where gas growth is enhanced by convective transfer in the aqueous phase. We find that modeling results in the transport-enhanced scenario match the experimental observations of gas bubble size distributions better.

Water relative permeability with exsolved CO_2 can be estimated with modeled gas distributions under different conditions. The estimated water relative permeability curves using modeling results in the transport-enhanced scenario agree well with our experimental measurements. For carbonated brine migrating up a fault slowly (an equivalent depletion rate of 5 kPa/day), with 5% exsolved gas, the water relative permeability is estimated to be 0.6~0.8 with various sandstones. Both the preferential growth in high velocity pore space and the poorly interconnected gas morphology lead to the disproportional reduction of water mobility.

CO_2 exsolution does not appear to create significant risks for storage security in geological carbon sequestration. Due to the low mobility of exsolved CO_2 and its large impact on reducing water flow, if carbonated brine migrates upwards and exsolution occurs, brine migration would be greatly reduced and limited by the presence of exsolved CO_2 and the consequent low relative permeability to brine. Similarly, if an exsolved CO_2 phase were to evolve in the seal, for example, after CO_2 injection stops, the effect would be to reduce the permeability to brine and the CO_2 would have very low mobility.

Acknowledgements

This work is funded by the Global Climate and Energy Project (GCEP) at Stanford University. This work was also supported by U.S. EPA, Science To Achieve Results (STAR) Program, Grant #: 834383, 2010-2012.

We thank William R. Wiley Environmental Molecular Sciences Laboratory, a United States Department of Energy scientific user facility operated by Pacific Northwest National Laboratory, and Advanced Light Source, operated by Lawrence Berkeley National Laboratory, for granting the user access to conduct experiments.

We appreciate collaborations with Prof. Ronald Falta in Department of Environmental Engineering and Earth Sciences at Clemson University; Dr. Changyong Zhang at Pacific Northwest National Laboratory; Dr. Jonathan Ajo-Franklin, Dr. Marco Voltolini and Dr. Jil Geller in Earth Sciences Division at Lawrence Berkeley National Laboratory.

More detailed information can be found in Dr. Zuo's Ph.D. dissertation, available through <http://searchworks.stanford.edu/view/10530951>.

References

- [1] Benson SM, Cook P. Underground Geological Storage. *IPCC Special Report on Carbon Dioxide Capture and Storage*, Chapter 5, Intergovernmental Panel on Climate Change, Cambridge University Press, Cambridge, U.K.; 2005.
- [2] Leonenko Y, Keith DW. Reservoir engineering to accelerate the dissolution of CO₂ stored in aquifers. *Environmental Science & Technology* 2008; 42(8): 2742-2747.
- [3] Enouy R, Li M, Ioannidis MA, Unger A. Gas exsolution and flow during supersaturated water injection in porous media: II. column experiments and continuum modeling. *Advances in Water Resources* 2011; 34(1):15-25.
- [4] Zuo L, Krevor SCM, Falta RW, Benson SM. An experimental study of CO₂ exsolution and relative permeability measurements during CO₂ saturated water depressurization. *Transport in Porous Media* 2012, 91(2):459-478.
- [5] Zuo L, Zhang C, Falta RW, Benson SM. Micromodel investigations of CO₂ exsolution from carbonated water in sedimentary rocks. *Advances in Water Resources* 2013, 53:188-197.
- [6] Luhmann AJ, Kong XZ, Tutolo BM, Ding K, Saar MO, Seyfried WEJ. Permeability reduction produced by grain reorganization and accumulation of exsolved CO₂ during geologic carbon sequestration: A new CO₂ trapping mechanism. *Environmental Science & Technology* 2012, 47(1):242-251.
- [7] Oldenburg CM, Pruess K, Benson SM. Process modeling of CO₂ injection into natural gas reservoirs for carbon sequestration and enhanced gas recovery. *Energy & Fuels* 2001, 15(2):293-298.
- [8] Falta RW, Zuo L, Benson SM. Migration of exsolved CO₂ following depressurization of saturated brines. *Greenhouse Gases: Science and Technology* 2013, 3(6):503-515.
- [9] Perrin JC, Benson SM. An experimental study on the influence of sub-core scale heterogeneities on CO₂ distribution in reservoir rocks. *Transport in Porous Media* 2010, 82(1):93-109.
- [10] Krevor SCM, Pini R, Zuo L, Benson SM. Multiphase flow properties of CO₂ and water in sandstone rocks at reservoir conditions. *Water Resources Research* 2012, 48(2):W02532.
- [11] Tsimpanogiannis IN, Yortsos YC. Model for the gas evolution in a porous medium driven by solute diffusion. *AIChE Journal* 2002, 48(11):2690-2710.
- [12] Silin D, Patzek T. Pore space morphology analysis using maximal inscribed spheres. *Physica A: Statistical Mechanics and its Applications* 2006, 371(2):336-360.